Mechanistic modelling of separating dispersions in pipes using model-based design of experiments techniques

Nikola Evripidou, Federico Galvanin [*], Panagiota Angeli [*]

ThAMeS Multiphase, Department of Chemical Engineering, University College London, London WC1E 7JE, United Kingdom

ARTICLE INFO

ABSTRACT

This work presents a parametric study on a mechanistic model for separating liquid–liquid dispersions in pipes. The model considers drop-settling, drop-interface coalescence and drop-drop coalescence, predicting the evolution of four characteristic layers during separation. Parameter estimation, parametric sensitivity analysis (PSA), and model-based design of experiments (MBDoE) techniques are employed to acquire precise parameter estimates and propose optimal experimental conditions, thereby enhancing the accuracy of existing models. Experimental data from literature using oil-in-water dispersions are used for parameter estimation. PSA reveals regions of high sensitivity of the model outputs to uncertain parameters, which are corresponding to favourable sampling locations. Manipulating the mixture velocity, the dispersed phase fraction, and the layer heights at the inlet influences these sensitive regions. Clustered measurements around highly sensitive regions in the pipe enhance the information content they provide. MBDoE demonstrates that either of the A-, D-, or E-optimal experimental design criteria improves the expected parameter precision.

1. Introduction

Dispersed pipe flows are common in many industrial processes and plants, with applications in areas such as chemical, pharmaceutical, and food processing. They can be used to enhance heat or mass transfer, by increasing the contact area between two or more substances. They are also encountered in the petroleum industry during the transportation of oil mixtures with water; they have been used to minimise pipe erosion by dispersing the water (Wang and Zhang, 2016) or frictional losses during transportation of heavy oils (Pilehvari et al., 1988). For initially dispersed flows, low mixture velocities can lead to gravity separation due to the density difference between the two phases. Gravity separation can in fact be exploited in the design of in-line separators. These are especially important in the oil and gas industries where they enable in-situ oil recovery and thus make extraction in older oil fields economically viable (Skjefstad and Stanko, 2019). In cases where dispersions are important, their tendency to separate can be detrimental.

Due to the complexity of dispersed pipe flows and the difficulties in obtaining direct measurements in industry, models play a crucial role in predicting and understanding their behaviour. Accurate models provide information that is critical for optimising the design and operation of industrial facilities and predicting the behaviour of the dispersed system

under different operating conditions or when different fluids are used. Mechanistic models in particular only consider the major separation mechanisms. They have the advantage of providing fast and accurate predictions, but their performance relies heavily on the precise estimation of their parameters. Unfortunately, obtaining precise parameter estimates for complex multiphase flow models through experimental means can be challenging, expensive, and time-consuming. Nevertheless, they are often preferred by industry to complex computational fluid dynamics simulations due to their ability to provide predictions quickly for extrapolation and scale-up.

Several mechanistic models have been developed for dispersion separation in batch settlers. Assuming an oil-in-water dispersion in a batch settler, separation begins with the formation of a pure water layer at the bottom of the settler as the oil drops begin to float upwards. Eventually, several drops reach the coalescing interface and accumulate into a dense-packed zone. Interfacial coalescence of drops with the pure oil layer results in an increase in the oil layer thickness. Frising et al. (2006) published a comprehensive review of the models available in literature for the prediction of the separation behaviour of batch liquid–liquid dispersions. The authors noted that these models can be broadly classified into two types: settling-based models and coalescence-based models. Settling-based models were mostly developed by
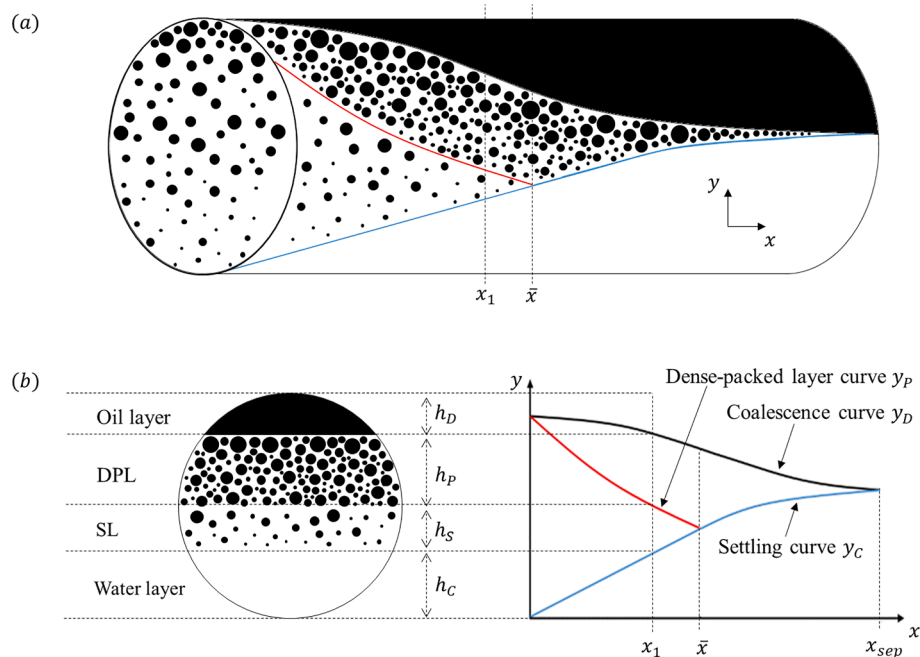

Fig. 1. (a) A schematic illustrating dispersion separation in a pipe along the axial dimension, (b) graph of the flow profile of the pipe and a schematic of the pipe cross section that shows the distinct layers at $x = x_1$.

Hartland and Jeelani and their colleagues (Balmelli et al., 2000; Bhardwaj and Hartland, 1994; Jeelani et al., 1990, 1999, 2005b, Jeelani and Hartland, 1986a, 1988, 1993; Mason et al., 1995; Panoussopoulos et al., 1997; Jeelani and Hartland, 1986b; Jeelani et al., 2005a), and assume that the separation process involves two main mechanisms, namely drop-settling and interfacial coalescence. On the other hand, coalescence-based models focus on small, non-deformable drops, and consider drop-drop coalescence as the primary separation mechanism (Lobo et al., 1993). Other models, such as those developed by Henschke et al. (2002) and Noik et al. (2013), comprehensively include all three separation mechanisms (i.e. settling, drop-drop coalescence, and drop-interface coalescence).

Subsequent studies extended the batch models to one-dimensional pipe flows (Pereyra et al., 2013; Evripidou et al., 2019), by considering the change in geometry and by utilizing the average mixture velocity to convert the time scale to a length scale. A more recent paper by Evripidou et al. (2022) identified cases where the rate of interfacial coalescence in pipes is larger than the rate of drop-settling, leading to a separation process that does not involve the formation of a dense-packed zone. The paper also presented a universal mechanistic model that provides predictions on the flow pattern development and separation of different dispersed pipe flows. The model, however, is reliant on two fitted parameters, namely a settling and a coalescence parameter. Obtaining precise estimations of the model parameters is critical, as they directly affect the accuracy of the predictions.

Precise parameter estimates can be challenging to obtain as the system may be affected by identifiability issues (Galvanin et al., 2013). Furthermore, it is usually impossible to fit the two parameters using industrially acquired data due to the scarcity of essential measurements required for parameter estimation, particularly measurements that entail the necessary level of detail, in many industrial settings. Additionally, limitations posed by the opaque test-sections and fluids, which restrict visual observations and hinder the use of several sampling methods, further exacerbate the difficulty. Instead, the necessary information can be obtained in pilot-scale laboratory experiments (Pereyra et al., 2013, Voulgaropoulos et al., 2019). Pilot-scale facilities, however, are often small in length and diameter; hence, the experiments must be carefully designed to ensure that the measurements provide

sufficient information for parameter estimation.

Several computational methods are available for parameter estimation. These methods either utilise existing experimental measurements or entail model-based experimental design to maximise the collection of information available for parameter estimation. *Parametric sensitivity analysis* (PSA) is a convenient tool that is utilised during experimental design, to understand the effect of parameters on the model responses (Saltelli et al., 2009). PSA helps to identify parametrically sensitive regions in a pipe, which are favourable sampling locations. A pipe region is said to be parametrically sensitive when a small variation in some of the uncertain model parameters leads to significant variations in one or more of the model outputs. Model-based design of experiments (MBDoE) methods can be used in addition to ensure that the designed experiment will maximize the information produced by the measurements.

Various MBDoE techniques have been suggested in the literature to design experiments that aim to improve the statistical precision of parameter estimates (Franceschini and Macchietto, 2008; Quaglio et al., 2019; Huang et al., 2023). Conventional MBDoE methods for parameter precision are based on the solution of an optimization problem where the objective function to maximize is a metric of expected information. The expected information for the estimation of the model parameters is evaluated through the Fisher Information Matrix (FIM) (Pukelsheim, 1993). The FIM is a measure of the sensitivity of the model responses to a variation in the values of model parameters (Walter and Pronzato, 1997). Typically, the experimental design metric being maximized is a scalar quantity of the *expected* FIM (Walter and Pronzato, 1997) which is the inverse of the variance–covariance matrix of model parameters. Popular experimental design metrics are the so-called alphabetical criteria (Pukelsheim, 1993) including FIM determinant (D-optimal criterion), trace (A-optimal criterion), minimum eigenvalue (E-optimal criterion), or ratio between maximum and minimum FIM eigenvalues (modified E-optimal). Once the experiment is performed, data are collected and the measurements are used in the parameter estimation problem to compute the observed FIM and characterise the variance of model parameters.

This work introduces a framework for estimating model parameters, evaluating their relative impact on model predictions through parametric sensitivity analysis, and providing guidance on optimal
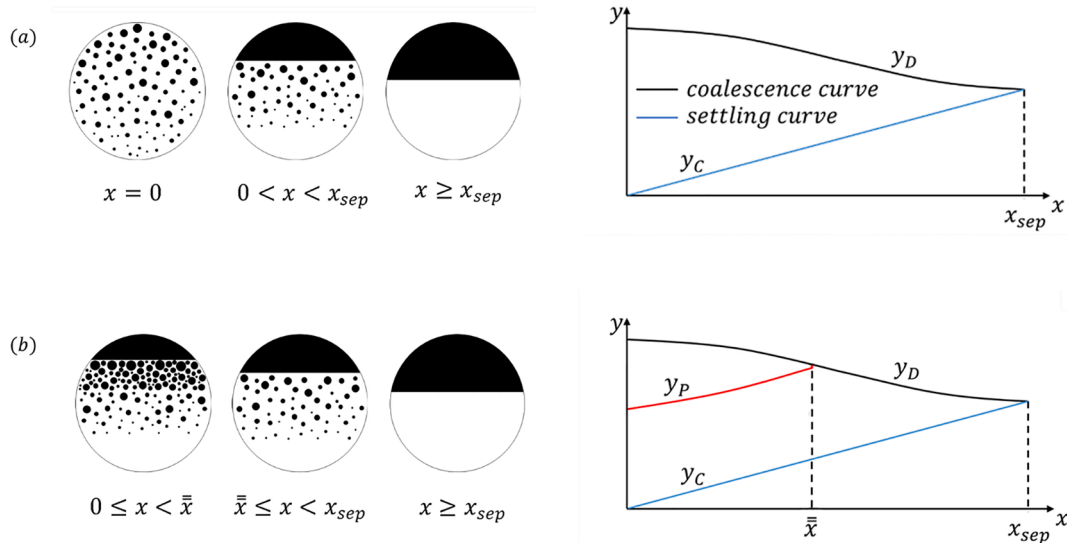
Fig. 2. Schematics illustrating the flow profiles and cross-sectional schematics of the pipe showcasing the flow pattern at different pipe lengths, in two different scenarios of settling-controlled dispersion separation.

experimental conditions to use in future experiments to obtain precise parameter estimates for mechanistic models of separating dispersed pipe flows. The proposed approach can be employed to determine optimal experimental configurations for pre-existing setups, as well as to devise novel experimental protocols from inception, with the objective of acquiring measurements that contain sufficient information for precise estimation of the parameters. To the best of our knowledge, this is the first time such a framework is being proposed for separating dispersed flows. The proposed framework includes 1) the calibration of the mechanistic model for separation of dispersed flows, 2) sensitivity analysis, and 3) model-based experimental design. Section 2 gives a brief overview of the proposed model while Section 3 discusses the experimental program from which the measurements were extracted. Section 4 outlines the methodology and Section 5 presents the obtained results. Throughout this work the gPROMS ModelBuilder is used.

2. Mechanistic model

The one-dimensional mechanistic model proposed by Evripidou et al. (2022) is considered, that predicts the separation of dispersions in horizontal pipes. Assuming a uniform oil-in-water dispersion is present at the pipe inlet, separation can lead to the formation of four distinct layers as shown in Fig. 1: a pure water layer at the bottom of the pipe, a settling layer (SL) which is dilute and where drop settling occurs, a dense-packed layer (DPL), and a pure oil layer at the top. The model accounts for the settling (flotation or sedimentation) of droplets, drop growth through binary drop coalescence in the packed layer, and interfacial coalescence of drops with their homophase.

The model requires knowledge of the fluid properties (i.e. densities, viscosities, and surface tension), the mixture velocity u_M, the dispersed-phase fraction φ_0, the intial thicknesses of the layers, and the average drop diameter at the pipe inlet $d_{p,0}$. In turn, it outputs the height y of each characteristic layer and the average drop diameter in the DPL along the pipe. In an oil-in-water dispersion, the height of the water layer from the bottom of the pipe y_C, is determined by the settling velocity of drops and is also known as the *settling (flotation/sedimentation) curve*. Conversely, the height of the oil layer y_D, is determined by the rate of drop-interface coalescence and is referred to as the *coalescence curve*. When the layer heights are plotted against pipe length, they provide the flow profiles. The flow profiles are graphical representations that illustrate the evolution of the characteristic layers along the pipe, with the *x*-axis denoting the axial displacement from the pipe inlet and the *y*-axis

representing the height from the bottom of the pipe. Fig. 1(a) shows a schematic illustrating dispersion separation in a pipe, while Fig. 1(b) presents the flow profile of the pipe, along with a schematic of the pipe cross section at $x = x_1$, showcasing the distinct layers.

Different flow patterns and flow pattern transitions can emerge from oil-in-water dispersed pipe flows, depending on the inlet conditions and the relative rates of drop settling and drop-interface coalescence. According to Evripidou et al. (2022), if the rate of drop settling is faster than the rate of drop-interface coalescence, coalescence-controlled separation occurs. Under these circumstances, the drops accumulate within a DPL underneath the pure oil layer, as shown in Fig. 1. Drop settling continues until the SL depletes at $x = \bar{x}$ (Fig, 1(b)). On the other hand, if the rate of drop settling is slower than the rate of drop-interface coalescence, drop settling will govern the separation rate along the entire pipe. In these instances, a DPL does not form, as illustrated in Fig. 2(a). If a DPL is present at the inlet, it may deplete if the rate of drop-interface coalescence is considerably faster than the rate of drop settling. The depletion of the DPL occurs at $x = \bar{\bar{x}}$, as depicted in Fig. 2(b). In all scenarios, the length at which complete separation of the two immiscible liquids is achieved ($x = x_{sep}$) is determined by the intersection of the *coalescence curve* y_D and the *settling curve* y_C.

For simplicity and ease of modelling, the model operates under certain assumptions. It assumes a constant velocity u_M across all layers in the spanwise direction, without considering velocity profiles or momentum exchange between the layers. It also assumes monodispersed layers, disregarding drop break-up, and considers the surface tension as constant.

Although in reality there is no apparent interface between the SL and the DPL, for modelling purposes, they are considered as two distinct layers, as shown in Figs. 1 and 2. The oil fraction, φ, within each layer is considered constant with height and a step-change in the oil fraction is assumed at the interface between the two layers. The SL oil fraction, φ_S, is presumed to be equal to the initial oil fraction of the mixture, φ_0, while the oil fraction of the DPL, φ_P, is calculated within the model.

The mechanistic model consists of three systems of differential algebraic equations (DAEs), with each system describing a different flow configuration (i.e. *4-layer, 3-layer with DPL, 3-layer with SL*). The main model equations are outlined below, while the complete model can be found in the Appendix.

Table 1

Model parameters.

Parameter	Description	Value	Unit	Reference
ρ_C	Density of water	998	kg m^{-3}	Perry et al. (1997)
ρ_D	Density of oil	857	kg m^{-3}	Pereyra et al. (2013)
μ_C	Viscosity of water	0.00089	Pa s	Perry et al. (1997)
μ_D	Viscosity of oil	0.027	Pa s	Pereyra et al. (2013)
γ	Surface tension	0.029	N m^{-1}	Pereyra et al. (2013)
g	Gravitational acceleration	9.81	m s^{-2}	Perry et al. (1997)
H	Hamaker coefficient	10^{-20}	N m	Pereyra et al. (2013)
C_h	Settling parameter	–	Dimensionless	–
r_V^*	Coalescence parameter	–	Dimensionless	–

2.1. Settling curve

For an oil-in-water dispersion, the settling curve y_C corresponds to the curve of the water layer thickness h_C. In the presence of a settling layer, i.e. for the *4-layer* flow regime depicted in Fig. 1(b) at $x = x_1$ and 2 (b) at $0 \leq x < \overline{\overline{x}}$, as well as the *3-layer with SL* flow regime illustrated in Fig. 2(a) at $0 < x < x_{sep}$ and 2(b) at $\overline{\overline{x}} \leq x < x_{sep}$, the setting curve is given by

$$\frac{dy_c}{dx} = \frac{dh_c}{dx} = \frac{u_S}{u_M}. \tag{1}$$

u_S is the settling velocity of drops in the SL and is given by

$$u_S = C_h \frac{3\lambda\varphi_S\mu_C}{C_w\xi(1-\varphi_S)\rho_C d_p} \left[\left(1 + Ar \frac{C_w\xi(1-\varphi_S)^3}{54\lambda^2\varphi_S^2} \right)^{0.5} - 1 \right], \tag{2}$$

where C_h is the hindered settling parameter and is one of the two uncertain parameters that must be obtained experimentally. The other parameters found in Eq. (2) are specified in Section A.2 of the Appendix.

In the case of depletion of the SL, specifically in the *3-layer with DPL* flow regime illustrated at $x \geq \overline{\overline{x}}$ in Fig. 1, the settling curve can be obtained through a mass balance, after estimating the thicknesses of the other layers, as follows

$$y_C = h_C = ID - h_P - h_D. \tag{3}$$

2.2. Coalescence curve

The coalescence curve gives the height of the oil interface from the bottom of the pipe, hence

$$y_D = ID - h_D. \tag{4}$$

The increase in the thickness of the oil layer h_D is determined by the drop-interface coalescence rate. Assuming monodispersed layers where coalescing drops have a diameter equal to $d_{p,I}$, the evolution of the oil layer is described by

$$\frac{dh_D}{dx} = \frac{2\varphi_I d_{p,I}}{3\tau_I u_M}, \tag{5}$$

where φ_I is the dispersed-phase fraction along the coalescing interface and is fixed at 0.9 as suggested by Evripidou et al. (2022), while τ_I is the

coalescence time between a drop and the interface.

The drop size evolution within the DPL is captured by

$$\frac{d(d_{p,I})}{dx} = \frac{d_{p,I}}{6\tau_C u_M} \tag{6}$$

where τ_C corresponds to the drop-drop coalescence time.

Finally, the drop-interface and the drop-drop coalescence times are given by

$$\tau_I = \frac{(6\pi)^{\frac{7}{6}}\mu_C \, r_a^{\frac{7}{3}}}{4\gamma^{\frac{5}{6}}\mathrm{H}^{\frac{1}{6}} r_{F,I} r_V^*}, \tag{7}$$

and

$$\tau_C = \frac{(6\pi)^{\frac{7}{6}}\mu_C \, r_a^{\frac{7}{3}}}{4\gamma^{\frac{5}{6}}\mathrm{H}^{\frac{1}{6}} r_{F,C} r_V^*}, \tag{8}$$

respectively. r_V^* is the coalescence parameter that needs to be determined through experiments. The remaining variables are defined in Section A.2 of the Appendix.

3. Experimental data

The experimental measurements of the *settling* and the *coalescence curves* from Pereyra et al. (2013) are used in this work. The experiments were conducted in a fully instrumented multiphase flow facility consisting of a transparent PVC pipe with an inner diameter (*ID*) equal to 0.1 m to allow visual observation of the distinct layers along the pipe. A static mixer was installed in series with the T-junction at the inlet of the test section to promote mixing of the two phases. Tap water and Tulco Tech 80 mineral oil were used as test fluids. The properties of the fluids are given in Table 1. The heights of the pure water layer y_C and the pure oil layer y_D were measured at five different locations along the pipe using measuring tapes. The readings of the measuring tapes were corrected to account for the effect of the pipe curvature. The experimental set-up and methods are described in detail in Pereyra et al. (2013).

4. Methodology

4.1. Parameter estimation

Parameter estimation is the process of calculating the values of the unknown parameters of a model from physical measurements. Only two parameters are unknown here, the settling parameter C_h and the coalescence parameter r_V^*. These are specific to each system and must be determined experimentally. C_h appears in the calculation of the drop settling velocity from Eq. (2) and accounts for hindrance in drop-settling due to the flow and droplet interactions. It also compensates for any uncertainty in the estimate of the average drop size at the inlet as shown by Evripidou et al. (2022). r_V^* is associated with coalescence and is used in Eqs. (7) and (8) in the calculation of the drop-drop and the drop-interface coalescence times.

The two parameters, C_h and r_V^*, were estimated using the *Model Validation* entity in gPROMS ModelBuilder. The values of other parameters used in the model were obtained from Pereyra et al. (2013) and Perry et al. (1997), whenever this was possible, and are summarised in Table 1. The remaining parameters which appear in Eq. (2) for the calculation of the settling velocity u_S, are obtained by the correlations in Section A.2 of the Appendix.

Model Validation in gPROMS is based on the Maximum Likelihood formulation. This is a linearization-based approach (Bard, 1977), which aims to determine the optimal values for the uncertain parameters and the associated probability distribution that best fits the experimental measurements. Within *Model Validation,* gPROMS conducts a Student's *t*-test to assess the precision of the parameter estimates. The *t*-value for

Table 2
Conditions of the experiments. (Pereyra et al., 2013).

Case	ID (m)	φ_0	u_M (m s^{-1})	$y_{C,0}$ (m)	$y_{D,0}$ (m)
1	0.1	0.40	0.06	0.025	0.1
2	0.1	0.40	0.09	0.025	0.1
3	0.1	0.40	0.13	0.025	0.1
4	0.1	0.60	0.09	0.016	0.1

the i-th model parameter is computed through Eq. (9).

$$t_i = \frac{\theta_i}{t(95\%, N - N_\theta)\sqrt{v_{\theta,i}}}, \tag{9}$$

where t_i is the 95% t-value of the i-th parameter, θ_i is the corresponding estimated value, and $v_{\theta,i}$ is its estimated variance (Bard, 1977). $t(95\%, N - N_\theta)$ is the reference t-value with a 95% confidence level and $(N - N_\theta)$ degrees of freedom obtained from statistical tables, where N is the total number of measurements and N_θ is the number of uncertain parameters to be estimated. 95% t-values larger than the reference t-value tend to indicate precise parameter estimates (Draper and Smith, 1998).

Finally, Eq. (10) gives the 95% confidence interval, *CI*. This interval represents the range within which the new parameter estimates would fall 95% of the time, when parameter estimation is repeated with new experimental data.

$$CI = t(95\%, N - N_\theta)\sqrt{v_{\theta,i}}. \tag{10}$$

C_h and r_V^* were estimated using experimental measurements of the *settling curve* y_C and the *coalescence curve* y_D. The variance of the experimental measurements of the layer heights was assumed to be constant, with a standard deviation σ of 0.01 m. The oil fraction and/or the mixture velocity varied between cases. The conditions of the cases included in the parameter estimation are outlined in Table 2, together with the initial heights of the *settling curve* $y_{C,0}$ and the *coalescence curve* $y_{D,0}$. The average drop size at the inlet $d_{p,0}$ was assumed to be independent to the mixture velocity u_M and the oil fraction φ_0 and equal to 0.0025 m for all cases.

Finally, in *Model Validation*, gPROMS also performs a χ^2 test to calculate the χ^2 value, which serves as a statistical measure to assess the goodness of fit between a model and the experimental (observed) data. This value is calculated by summing the squared differences between the observed and expected values, and it is often used in hypothesis testing to determine whether a model adequately fits the data (Hines et al., 2003). A good fit between the model and experimental data is indicated when the calculated χ^2 value is lower than the critical χ^2 value, which is obtained from the χ^2-squared distribution table based on the chosen significance level and degrees of freedom for the hypothesis test.

4.2. Parametric sensitivity analysis (PSA)

PSA serves as a valuable tool for identifying the pipe locations where the model outputs, such as the *settling curve* y_C and the *coalescence curve* y_D, exhibit the highest sensitivity to the uncertain parameters. This method is based on simplistic local linearization, and while more advanced methods exist in the literature (Joshi et al., 2006; Schenkendorf et al., 2018; Krausch et al., 2019), a local linearization works well in cases where there is a preliminary knowledge on the values of model parameters. By pinpointing areas of heightened sensitivity, the optimal sampling locations are determined. Measurements at these selected locations subsequently provide invaluable information for fitting the uncertain parameters with high precision.

The first-order local sensitivity $s_{\theta_i}^y$, or simply *local sensitivity*, of a dependent variable y with respect to the input parameter θ_i is defined as $s_{\theta_i}^y = \frac{\partial y}{\partial \theta_i}$, where s is also known as the *absolute sensitivity*. The absolute

sensitivity can be obtained by calculating the change in output y arising from an infinitesimally small perturbation ε in parameter θ_i, i.e.:

$$\frac{\partial y}{\partial \theta_i} \approx \frac{\Delta y}{\Delta \theta_i} \approx \frac{y_i' - y_i}{\theta_i(1 + \varepsilon) - \theta_i}. \tag{11}$$

Noting here that the approximation error is of the order of ε. The accuracy of the computations can be increased further by using a second-order approximation that decreases the error to the order of ε^2.

The local sensitivities of N dependent variables (outputs) to n input model parameters can be expressed in the form of a sensitivity matrix, **Q**

$$\mathbf{Q}(\boldsymbol{\phi}, \boldsymbol{\theta}) = \begin{bmatrix} \frac{\partial y_1}{\partial \theta_1} & \cdots & \frac{\partial y_1}{\partial \theta_n} \\ \vdots & \ddots & \vdots \\ \frac{\partial y_N}{\partial \theta_1} & \cdots & \frac{\partial y_N}{\partial \theta_n} \end{bmatrix} \approx \begin{bmatrix} \frac{y_1' - y_1}{(\theta_1 + \varepsilon) - \theta_1} & \cdots & \frac{y_1' - y_1}{(\theta_n + \varepsilon) - \theta_n} \\ \vdots & \ddots & \vdots \\ \frac{y_N' - y_N}{(\theta_1 + \varepsilon) - \theta_1} & \cdots & \frac{y_N' - y_N}{(\theta_n + \varepsilon) - \theta_n} \end{bmatrix}, \tag{12}$$

where $\boldsymbol{\theta}$ is the N_θ-dimensional set of estimated model parameters, C_h and r_V^*, and $\boldsymbol{\phi} = [ID, \varphi_0, u_M, y_{C,0}, y_{D,0}]$ is the experimental design vector. The experimental design vector $\boldsymbol{\phi}$ consists of all the control variables that can be manipulated and optimised during an experiment. Later in section 4.3, where an optimal experiment for dispersion separation in a pipe is being designed, the values of the control variables that maximise the expected information content of the experimental measurements are determined and collected in the optimal design vector $\boldsymbol{\phi_{opt}}$.

The Fisher Information Matrix (FIM) $\mathbf{H}_\theta$ takes the form

$$\mathbf{H_\theta}(\boldsymbol{\phi}, \boldsymbol{\theta}) = \mathbf{Q^T}\boldsymbol{\Sigma_y^{-1}}\mathbf{Q}, \tag{13}$$

where $\boldsymbol{\Sigma_y^{-1}}$ is the inverse variance–covariance matrix of measurement errors.

To quantify the combined sensitivity of the model outputs to the uncertain (independent) parameters, the multidimensional nature of the FIM $\mathbf{H_\theta}$ can be summarised by a scalar measure ψ. This is essentially a single scalar quantity that combines the local sensitivities of the model responses to variations in the values of the uncertain parameters. The trace $\mathrm{Tr}(\mathbf{H_\theta})$, the determinant $\mathrm{Det}(\mathbf{H_\theta})$, and the largest eigenvalue are all popular options for ψ (Pukelsheim, 1993) and are used in the alphabetic criteria discussed further in Section 4.3. In this work, the trace of the FIM is used for PSA, which represents the sum of squared sensitivities and exhibits a direct relationship with the sensitivities. $\mathrm{Tr}(\mathbf{H_\theta})$ is defined as

$$\psi = \mathrm{Tr}(\mathbf{H_\theta}) = \sum_i \sum_j \sigma_{jj}^{-2} \left(\frac{\partial y_j}{\partial \theta_i}\right)^2. \tag{14}$$

where σ_{jj} is the j-th diagonal element of $\boldsymbol{\Sigma_y}$.

In the model developed here, the trace of the FIM is a function of pipe length. The pipe profile of the sensitivity can be obtained by plotting $\mathrm{Tr}(\mathbf{H_\theta})$ against x, enabling the identification of the pipe locations that are the most sensitive to the uncertain parameters. In the model, the uncertain parameters C_h and r_V^* affect the rates of drop settling and coalescence, hence the heights of the layers along the pipe. A PSA was performed to determine the pipe locations where the *settling curve* y_C and the *coalescence curve* y_D (i.e. the model outputs that are measured in the relevant experimental set-up) are the most sensitive to C_h and r_V^* for the cases listed in Table 2. The model was executed three times, initially with the parameter estimates obtained during parameter estimation, then with a perturbation ε of 1% applied to C_h only, and finally with a perturbation ε of 1% applied to r_V^* only. The specific equations used in PSA are listed in section A.3 of the Appendix.

4.3. Experimental design for parameter precision

Physical experiments play a crucial role in enhancing the understanding of the separation mechanisms and improving the accuracy of

Table 3

Parameter estimation initial guesses, results, and statistical measures based on the *t*-test (parameters failing the *t*-test are indicated in boldface).

Model parameter	Initial guess	Lower & upper bounds	Final value	95% Confidence interval	95% *t*-value
C_h	0.15	0.1–1	0.1982	0.1321	**1.5**
r_V^*	0.007	0.001–0.015	0.0074	0.0028	2.7
				Reference *t*-value (95%):	1.7

the model. However, the experimental conditions and the measuring locations can significantly affect the quality of the information provided by experimental measurements. MBDoE for parameter precision involves the use of current knowledge about the model, such as the model structure and preliminary parameter estimates, in order to design experiments that minimise the uncertainty in the parameter estimates. This requires to mathematically quantify the parameter estimate uncertainty in scalar form. Common approaches are the so-called alphabetic criteria described below, which are all measures of the covariance matrix $\mathbf{V_\theta}(\boldsymbol{\phi}, \boldsymbol{\theta})$.

- The A-optimal criterion aims to minimise the trace of the covariance matrix, $\mathrm{Tr}(\mathbf{H_\theta})$.
- The D-optimal criterion aims to minimise the determinant of the covariance matrix $\mathrm{Det}(\mathbf{H_\theta})$.
- The E-optimal criterion aims to minimise the largest eigenvalue of the covariance matrix.

The alphabetic criteria are used to optimise experimental design by determining the optimal experimental conditions and measuring locations, thereby maximizing the information held by the experimental measurements that can be used in the estimation of the model parameters. MBDoE can be performed using the *Experiment Design* module in gPROMS ModelBuilder. This is an optimisation problem that aims to find the design vector $\boldsymbol{\phi}$ values, that minimise the chosen scalar measure of the expected variance–covariance matrix $\mathbf{V_{\theta,expected}}(\boldsymbol{\phi}, \boldsymbol{\theta})$, as shown in eqn (15).

$$\boldsymbol{\phi_{opt}} = \underset{\boldsymbol{\phi}}{argmin}\psi\left(\mathbf{V_{\theta,expected}}(\boldsymbol{\phi}, \boldsymbol{\theta})\right). \tag{15}$$

In Eq. (15), $\boldsymbol{\phi_{opt}}$ is the set of optimal experimental conditions and measuring locations and $\mathbf{V_{\theta,expected}}(\boldsymbol{\phi}, \boldsymbol{\theta})$ is the expected variance covariance matrix, which can be approximated (using the first term Taylor expansion) by the inverse of the expected FIM, $\mathbf{H_\theta}$.

$$\mathbf{V_{\theta,expected}}(\boldsymbol{\phi}, \boldsymbol{\theta}) \approx \mathbf{H_{expected}}(\boldsymbol{\phi}, \boldsymbol{\theta})^{-1}. \tag{16}$$

To perform MBDoE for parameter precision in gPROMS ModelBuilder, initial guesses for the uncertain parameters must be provided. These guesses can be based on parameter estimates either from existing literature for similar liquid–liquid systems or from initial experiments conducted specifically for this purpose. Initial guesses, as well as lower and upper bounds are also needed for the necessary length of the test section, the initial heights of the settling curve $y_{C,0}$ and the coalescence curve $y_{D,0}$, the average drop diameter at the inlet $d_{p,0}$, and the controlled experimental variables (i.e. the inner diameter of the pipe *ID*, the oil fraction φ_0, and the mixture velocity u_M). gPROMS then determines the necessary pipe length of the test section x_{pipe}, the optimal initial conditions ($h_{C,0}, h_{D,0}, d_{p,0}$), and the optimal settings of the controlled variables (ID, φ_0, u_M) that fall between these bounds. The variables that will be measured during the experiments must be defined under the Measurement and Sensors tab. The frequency or the location of the measurements must also be specified.

The expected improvement in the parameter estimates can be visualised through the confidence ellipses given by Eqs. (17) and (18) for $0 \leq \vartheta \leq \pi$.

$$x = \theta_1 + \mathbf{E}_{1,1}cos\vartheta + \mathbf{E}_{1,2}sin\vartheta \tag{17}$$

$$y = \theta_2 + \mathbf{E}_{2,1}cos\vartheta + \mathbf{E}_{2,2}sin\vartheta \tag{18}$$

Here, $\mathbf{E}$ is defined as

$$\mathbf{E} = \mathbf{v} \bullet \sqrt{\mathbf{D}} \bullet sf \tag{19}$$

where $\mathbf{v}$ is the matrix of eigenvectors and $\mathbf{D}$ is the matrix of eigenvalues of the variance–covariance matrix, and *sf* denotes a scaling factor determined by the chosen confidence level.

5. Results

5.1. Parameter estimation

Parameter estimation was performed using the *Model Validation* entity in gPROMS ModelBuilder for the four cases listed in Table 2. Table 3 presents the parameter estimation results, as well as statistical measures based on the *t*-test that are used to evaluate the accuracy and reliability of the model predictions. The table encompasses the initial guesses of the parameter values, the lower and upper bounds for each parameter, the final parameter estimates, the distance to the bounds of the respective 95% confidence interval, the 95% *t*-value for each parameter, and a reference 95% *t*-value. A 95% *t*-value for a parameter smaller than the reference *t*-value indicates that the information in the available data set is not sufficient to estimate this parameter precisely (Draper and Smith, 1998).

A weak negative correlation of -0.16 was observed between C_h and r_V^*. The 95% *t*-value for r_V^* is larger than the reference *t*-value, indicating that the coalescence parameter was estimated with sufficient precision. On the other hand, the 95% *t*-value for C_h is smaller than the reference *t*-value, suggesting that higher uncertainty is associated with the parameter estimate and that the estimate is not statistically significant. Further investigation is required to determine whether the uncertainty in C_h significantly affects the accuracy of the model. Although the model validation was repeated with different initial guesses and upper and lower bounds, they resulted in poorer fits with the experimental data.

5.1.1. Flow profiles

The flow profiles predicted by the model using the parameter estimates from Table 3 are illustrated in Fig. 3. These profiles correspond to the four cases specified in Table 2. To facilitate comparison of the model predictions to experiments, the figure also includes experimental measurements along with error bars of 0.01 m.

The four distinct flow profiles in Fig. 3 were obtained under varying operating and initial conditions. In each case, the thickness of the DPL decreases along the length of the pipe, indicating a coalescence rate that exceeds the settling rate. This observation suggests a separation process predominantly controlled by settling, ultimately leading to the depletion of the DPL. Within Cases 1–3, the flow profiles demonstrate that an increase in the mixture velocity u_M while maintaining other controlled variables and initial conditions constant, leads to slower separation and an increase in the separation length, x_{sep}. Moreover, the point of depletion of the DPL, $\overline{\overline{x}}$, moves further downstream from the inlet, as a response to the increase in the mixture velocity. A comparison between Cases 2 and 4 suggests that the dispersed phase fraction, φ_0, has a small effect on $\overline{\overline{x}}$. Following the depletion of the DPL, slower separation is observed at the larger oil fraction. Nevertheless, the relationship between the oil fraction and the rate of separation cannot be clearly established with the current data. This is due to the fact that in the conducted experiments, the change in the oil fraction φ_0 was accompanied by concurrent changes in the initial layer heights.
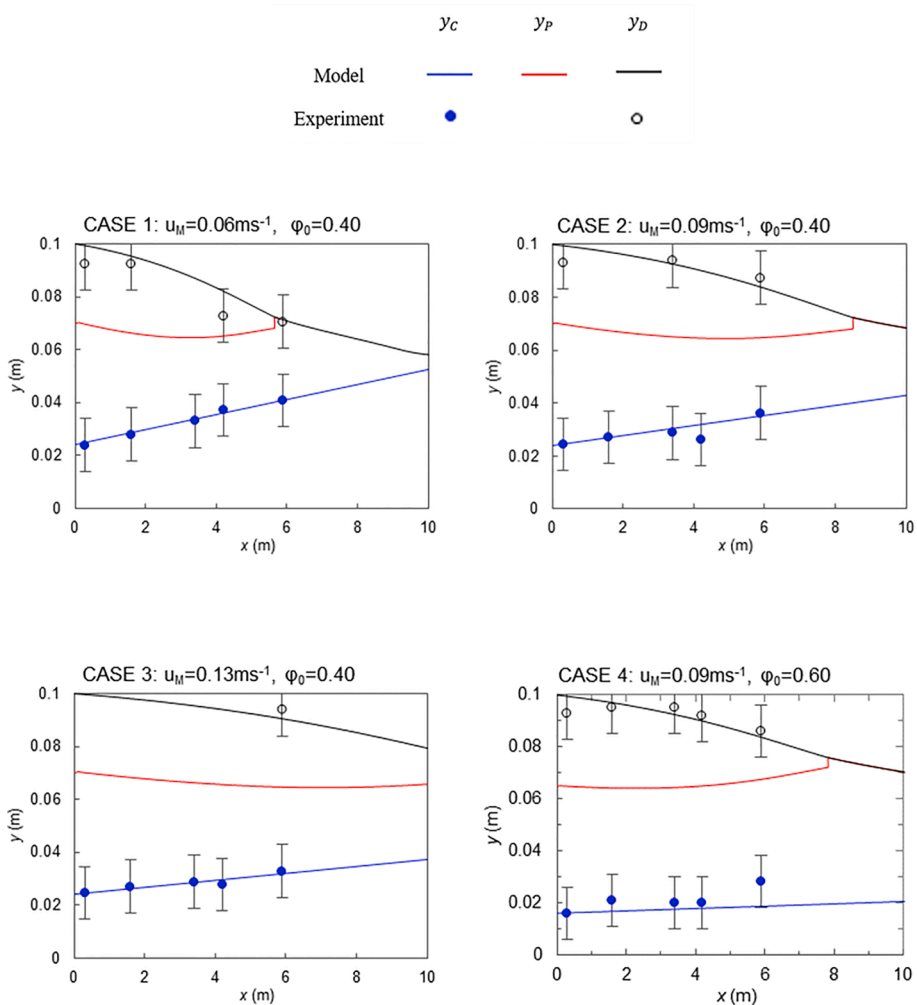
Fig. 3. Flow profiles obtained using the parameters estimates in Table 3 and experimental measurements of the coalescence and the settling curves with error bars of ± 1 cm.

Table 4
χ^2 values for the two measured responses obtained using the estimated parameters.

	Case 1		Case 2		Case 3		Case 4		Overall	
	χ^2	χ^2-crit.	χ^2	χ^2-crit.	χ^2	χ^2-crit.	χ^2	χ^2-crit.	χ^2	χ^2-crit.
y_C	0.023	6.0	0.39	6.0	0.052	7.8	1.2	7.8	1.6	26
y_D	1.4	6.0	0.55	3.8	–	–	0.61	7.8	2.6	20
Total	1.4	13	0.94	11	0.17	9.5	1.8	16	4.2	43

5.1.2. Goodness-of-fit

Table 4 shows the χ^2 values computed from the residuals for the settling curve, y_C, and the coalescence curve, y_D, across all cases using the model with the parameter estimates from Table 3, as well as the overall χ^2 values for each case and the overall χ^2 value for this model.. It is evident that all χ^2 values fall below the critical χ^2 values. The lack of a χ^2 value based on the residuals for the coalescence curve y_D for Case 3 can be attributed to the fact that only a single measurement was taken at these conditions. This leads to a situation where the number of measurements (1) is lower than the number of estimated parameters (2), and the problem is underspecified. Despite this limitation, the overall χ^2 value for this model is significantly lower than the critical χ^2 value. This indicates a strong agreement between the experimental data and the model predictions obtained using the parameter estimates from Table 3.

5.1.3. Effect of C_h on flow profile

As previously noted, the results in Table 3 reveal that the t-value associated with the hindered settling parameter C_h is lower than the reference t-value, indicating a failure of the t-test. This discrepancy suggests that the estimated value of C_h is characterized by higher uncertainty when compared to the coalescence parameter r_V^*. To investigate whether this uncertainty in C_h has a significant effect on the accuracy of the model, the simulations were repeated twice. In each simulation, the lower and upper bounds of the 95% confidence interval of C_h were utilised. These bounds were obtained by adding/subtracting the corresponding value for the 95% confidence interval from Table 3 to the parameter estimate, resulting in $C_{h,0.05} = 0.07$ and $C_{h,0.95} = 0.33$, respectively.

The hindered settling parameter C_h plays a critical role in determining the point of depletion of the DPL. As the DPL depletes, the effect of C_h on separation becomes even more pronounced, with drop-settling
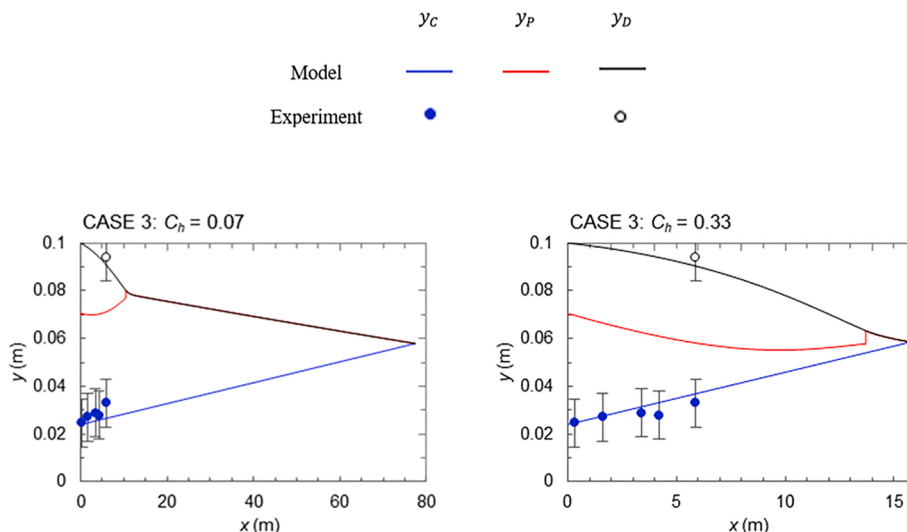
Fig. 4. Flow profiles of Case 3 ($u_M = 0.13\,\mathrm{m\,s^{-1}}$, $\varphi_0 = 0.40$) at the endpoints of the 95% confidence interval of C_h and experimental measurements of the coalescence and the settling curves with error bars of $\pm$ 1 cm.

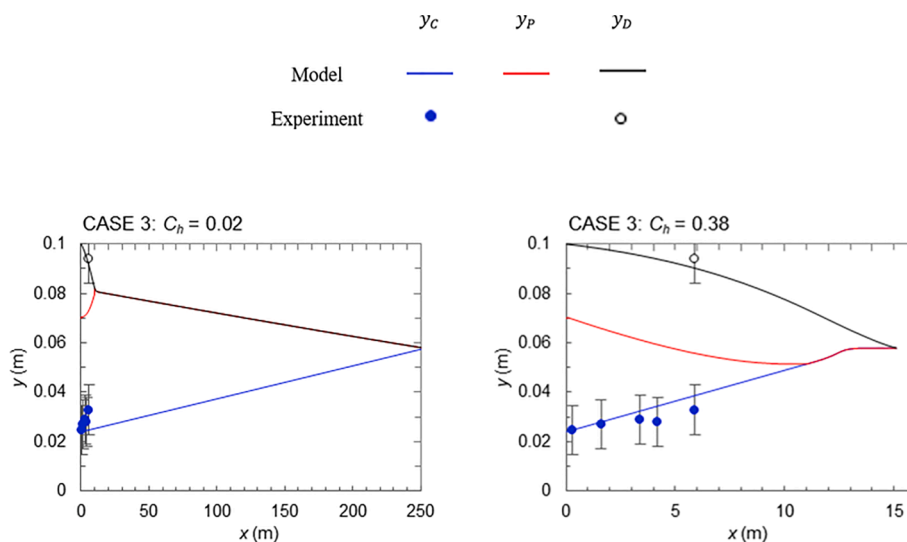**Fig. 5.** Flow profiles of Case 3 ($u_M = 0.13\,\mathrm{m\,s^{-1}}$, $\varphi_0 = 0.40$) at the endpoints of the 99% confidence interval of C_h and experimental measurements of the coalescence and the settling curves with error bars of ±1 cm.
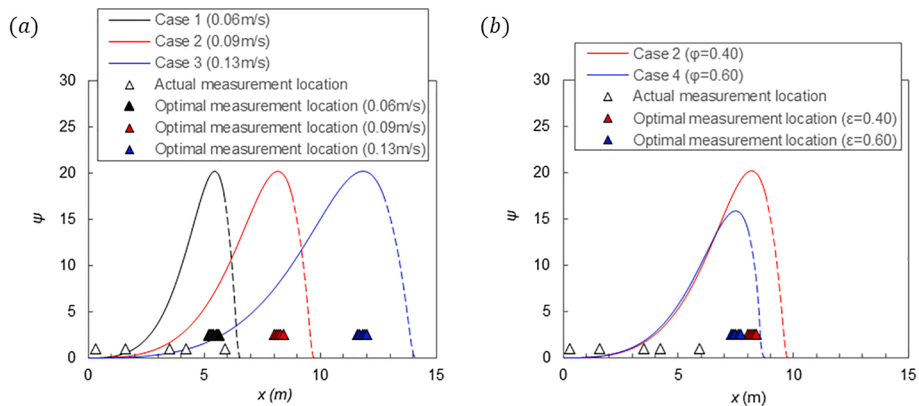

Fig. 6. Pipe profiles of the trace of the FIM of the four cases listed in Table 2. Subfigure (a) demonstrates the effect of the mixture velocity at a constant oil fraction of 0.40, while subfigure (b) illustrates the effect of the oil fraction at a constant mixture velocity of $0.09\,\mathrm{m\,s^{-1}}$.

Table 5

Initial guesses, and lower and upper bounds of the time-invariant controlled variables and the initial conditions used for MBDoE and optimal values obtained with each of the A-, D-, and E-optimal criteria.

Control variable	Final value			Initial value	Variable type	Lower bound	Upper bound
	A	D	E				
ID (m)	0.1	0.1	0.1	0.1	Fixed	–	–
φ_0	0.221	0.222	0.220	0.4	TBD	0.1	0.6
u_M(m s^{-1})	0.0760	0.0759	0.0762	0.06	TBD	0.03	0.3

Initial condition	Final value			Initial value	Variable type	Lower bound	Upper bound
	A	D	E				
$d_{p,0}$(mm)	0.25	0.25	0.25	0.25	Fixed	–	–
$h_{C,0}$(m)	0.0314	0.0314	0.0314	0.024	TBD	0	0.1
$h_{D,0}$(m)	0.0	0.0	0.0	0.0	TBD	0	0.1

Table 6

Optimal measurement locations obtained during MBDoE using each of the A-, D-, and E-optimal experimental design criteria.

Measurement location from pipe inlet (m)			
Initial guess	Optimal location		
	A	D	E
0.3	5.6	5.6	5.6
1.6	5.7	5.7	5.7
3.5	5.8	5.8	5.8
4.2	5.9	5.9	5.9
5.0	6.0	6.0	6.0

Table 7

Parameter statistics obtained during MBDoE using each of the A-, D-, and E-optimal criteria.

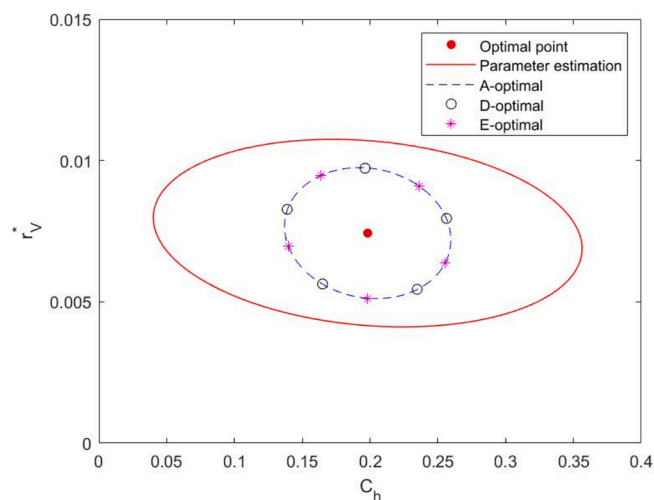| Parameter	Value	A-criterion		D-criterion		E-criterion	
		95% CI	95% t-value	95% CI	95% t-value	95% CI	95% t-value
C_h	0.1982	0.0507	3.91	0.0508	3.90	0.0506	3.92
r_V^*	0.0074	0.0019	3.88	0.0019	3.89	0.0019	3.87
						Reference t-value (95%):	1.68

Fig. 7. Plot illustrating the 95% confidence ellipses for C_h and r_V^* obtained from the initial parameter estimates and after MBDoE using A-, D-, and E-optimal criteria.

in the SL becoming the dominant mechanism governing separation.

Fig. 4 presents the predicted flow profiles of Case 3 at the endpoints of the 95% confidence interval of C_h. This visual representation effectively captures the potential variability and the significance of parameter uncertainty, providing valuable insights into the flow behaviour and separation dynamics within the system.

The results clearly demonstrate that the hindered settling parameter C_h has a substantial impact on the expected flow profile and the separation length. Although DPL depletion occurs between 10 m and 15 m for both cases, the prediction based on $C_{h,0.05}$ indicates a separation length that is nearly five times larger compared to that projected by $C_{h,0.95}$. This significant disparity between the two flow profiles highlights the need for higher precision in the estimation of C_h to ensure reliable and accurate model predictions.

The significance of the hindered settling parameter C_h becomes even more apparent when considering the wider 99% confidence interval. Fig. 5 presents the results obtained from the boundaries of the 99% confidence interval. At the lower bound, the DPL depletes similarly to previous cases. Conversely, at the upper bound, the SL depletes while the DPL persists until the two phases completely separate. This observation signifies a transition in the type of separation, shifting from a settling-controlled to a coalescence-controlled separation. Notably, the total separation length estimated using $C_{h,0.01}$ is more than 15 times greater compared to that predicted by $C_{h,0.99}$.

The influence of parameter r_V^* on model predictions has also been examined. Fig. A.2 of the Appendix illustrates the influence of r_V^* on the flow profiles of Case 3 at the endpoints of the 95% confidence interval. The analysis led to the conclusion that the influence of r_V^* on the performance of the model is relatively insignificant.

The findings depicted in Figs. 4 and 5 emphasise the considerable impact of parameter uncertainty in the estimation of C_h. New experimental data collected at regions of high sensitivity could be useful in increasing the precision of the estimate for this parameter. By focusing on these specific areas, the uncertainty associated with C_h can be reduced, thereby improving the accuracy of the model and enhancing the reliability of its predictions.

5.2. Parametric sensitivity analysis (PSA)

A PSA was performed to identify the pipe lengths with the highest sensitivity of the model responses to the uncertain parameters. Measurements taken at the locations of highest sensitivity hold the most information for the estimation of the uncertain parameters. The mechanistic model was solved for the parameter estimates obtained from parameter estimation θ_i and for $\theta_i(1 + \varepsilon)$, where ε is a small perturbation on the parameter of magnitude equal to 1%, to compute the absolute sensitivities for the water and the oil layer heights $s_{\theta_i}^{y_j}$ with respect to the uncertain parameters C_h and r_V^*.

Fig. 6 plots the trace of the FIM against pipe length and shows how

Table A.3

Model equations.

Dispersion separation: 4-layer flow regime

Settling

$$\frac{dh_c}{dx} = \frac{u_S}{u_M}$$

$$u_S = C_h \frac{3\lambda\varphi_0\mu_C}{C_w\xi(1-\varphi_o)\rho_C d_p} \left[\left(1 + Ar\frac{C_w\xi(1-\varphi_0)^3}{54\lambda^2\varphi_0^2} \right)^{0.5} - 1 \right]$$

$$Ar = \frac{\rho_C\Delta\rho g d_p^3}{\mu_C^2}$$

$$C_w = \frac{Ar}{6Re_\infty^2} - \frac{3}{K_{HR}Re_\infty}$$

$$K_{HR} = \frac{3(\mu_C+\mu_D)}{2\mu_C+3\mu_D}$$

$$Re_\infty = \frac{\rho_C u_{s,\infty} d_p}{\mu_C} = 9.72\left[(1+0.01Ar)^{\frac{4}{7}} - 1\right]$$

$$\lambda = \frac{1-\varphi_F}{2\varphi_F K_{HR}}\exp\left(\frac{2.5\varphi_S}{1-0.61\varphi_S}\right)$$

$$\xi = 5K_{HR}^{-\frac{3}{2}}\left(\frac{\varphi_S}{1-\varphi_S}\right)^{0.45}$$

Coalescence

$$\frac{dh_D}{dx} = \frac{2\varphi_I d_{p,I}}{3\tau_I u_M}$$

$$u_M\frac{d(d_{p,I})}{dx} = \frac{d_{p,I}}{6\tau_C}$$

$$\tau_I = \frac{(6\pi)^{\frac{7}{6}}\mu_C r_a^{\frac{7}{3}}}{4\gamma^{\frac{5}{6}}H^{\frac{1}{6}}r_{F,I}r_V^*}$$

$$\tau_C = \frac{(6\pi)^{\frac{7}{6}}\mu_C r_a^{\frac{7}{3}}}{4\gamma^{\frac{5}{6}}H^{\frac{1}{6}}r_{F,C}r_V^*}$$

$$r_{F,C} = 0.3025 d_{p,I}\sqrt{1-\frac{4.7}{La+4.7}}$$

$$r_{F,I} = \sqrt{3}r_{F,C}$$

$$r_a = 0.5 d_{p,I}\left(1-\sqrt{1-\frac{4.7}{La+4.7}}\right)$$

$$La = \left(\frac{|\rho_C-\rho_D|g}{\sigma}\right)^{0.6}\tilde{h}_P^{0.2}d_{p,I}$$

$$\tilde{h}_P = h_P$$

Settling layer oil fraction (if the inlet is partially separated)

$$\varphi_S = \frac{A_{pipe}\varphi_0 - A_{D,0} - A_{P,0}\varphi_{P,0}}{A_{S,0}}$$

Interface oil fraction

$$\varphi_I = 0.9$$

DPL area

$$A_P = \frac{A_{pipe}(\varphi_0-\varphi_S) - A_D(1-\varphi_S) + A_C}{\varphi_P-\varphi_S}$$

DPL oil fraction

$$\varphi_P = \frac{\varphi_S+\varphi_I}{2}$$

Geometric equations

$$A_C = \frac{ID^2}{4}\left[\pi - \cos^{-1}(\omega_C) + (\omega_C)\sqrt{1-\omega_C^2}\right]$$

$$\omega_C = \frac{2h_C}{ID} - 1$$

$$A_D = \frac{ID^2}{4}\left[\pi - \cos^{-1}(\omega_D) + (\omega_D)\sqrt{1-\omega_D^2}\right]$$

$$\omega_D = \frac{2h_D}{ID} - 1$$

$$\frac{\partial A_D}{\partial h_D} = 2\sqrt{h_D(ID-h_D)}$$

$$A_P = \frac{ID^2}{4}\left[\pi - \cos^{-1}(\omega_D) + (\omega_D)\sqrt{1-\omega_D^2}\right] - A_D$$

$$\omega_P = \frac{2h_P}{ID} - 1$$

$$\frac{\partial A_P}{\partial h_P} = 2\sqrt{(h_D+h_P)(ID-h_P-h_D)}.$$

$$\frac{\partial A_P}{\partial h_D} = \frac{\partial A_P}{\partial h_P} - \frac{\partial A_D}{\partial h_D} = 2\sqrt{(h_D+h_P)(ID-h_P-h_D)} - 2\sqrt{h_D(ID-h_D)}$$

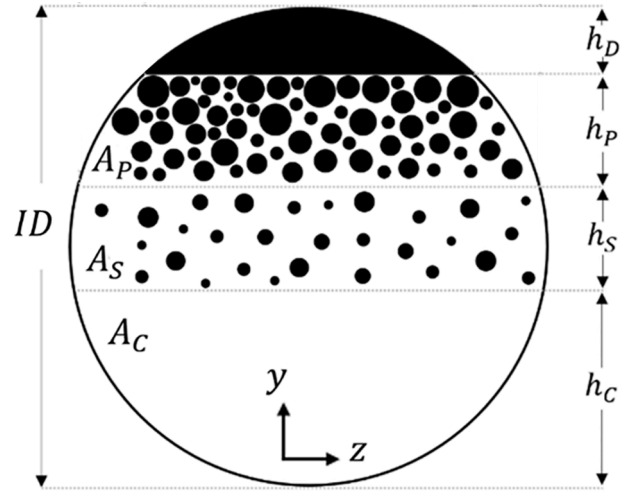$$A_S = ID - A_D - A_C - A_P$$

Fig. A.1. Schematic of the cross-section of a pipe with oil-in-water dispersed flow.

the combined sensitivity of the settling and the coalescence curves to both C_h and r_V^* changes along the pipe, for the four cases listed in Table 2. During PSA, only the 4-layer flow regime was studied to ensure that both settling and coalescence occur, thus enabling the estimation of both the settling and the coalescence parameters at the same time. The solid lines in Fig. 6 represent the trace of the FIM in the 4-layer flow regime. The simulations were allowed to continue beyond the point of DPL depletion, and for those specific lengths, ψ is depicted in the plots using dashed lines. The plot also includes the actual measurement locations used in the experiments performed by Pereyra et al. (2013), along with the optimal measurement locations for each case that maximise the information available for parameter estimation.

The plot in Fig. 6(a) compares Cases 1–3, to determine the effect of the mixture velocity on the sensitivity ψ, while other controlled variables (i.e. fluid properties, oil fraction, and pipe diameter) and initial conditions (i.e. initial layer heights and drop size at the inlet) remain unchanged. An increase in the mixture velocity from 0.06 m s^{-1} in Case 1 to 0.13 m s^{-1} in Case 3, moves the peak in the *sensitivity curve, ψ_{max}*, away from the inlet. Despite the shift in the location of the peak, the magnitude of ψ_{max} remains unchanged regardless of the mixture velocity. The results suggest that experiments performed at lower mixture velocities can provide the same amount of information in shorter test sections, as long as the other controlled variables and initial conditions remain unchanged.

Fig. 6(b) aims to examine the impact of the dispersed phase fraction on the combined sensitivity of the model outputs to the two uncertain parameters by comparing Cases 2 and 4. The fluid properties, the mixture velocity, the pipe diameter, and the drop size at the inlet are maintained constant between the two cases, however a variation in the layer heights at the inlet is observed. Notably, the increase in the oil fraction from 0.40 in Case 2 to 0.60 in Case 4 decreases the magnitude of the peak ψ_{max} but only slightly shift it towards the pipe inlet. These findings suggest that employing a lower dispersed phase fraction can enhance the available information for parameter estimation in the measurements. Nonetheless, it remains uncertain whether these observed changes resulted from the change in the oil fraction alone.

Finally, the findings presented in Fig. 6 indicate that the actual measurement locations employed in the experiments are suboptimal for parameter estimation, as they include measurements taken at locations characterised by low sensitivity. Fig. 6 provides valuable insights into the importance of optimizing measurement locations. By strategically refining the measurement locations, specifically by taking measurements at smaller intervals around ψ_{max}, the information content of the collected data will be substantially increased. This highlights the
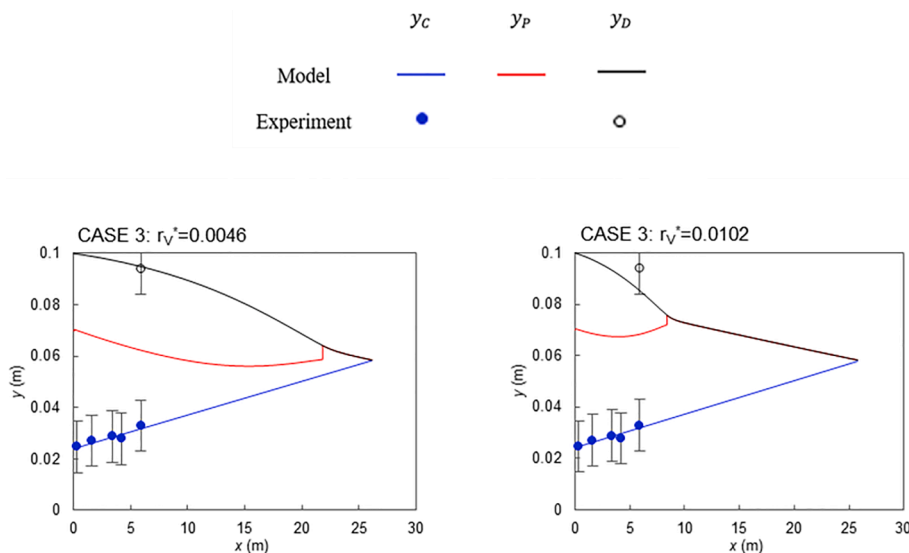
Fig. A.2. Flow profiles of Case 3 ($u_M = 0.13 \, \text{m s}^{-1}$, $\varphi_0 = 0.40$) at the endpoints of the 95% confidence interval of r_V^* and experimental measurements of the coalescence and the settling curves with error bars of $\pm$ 1 cm.
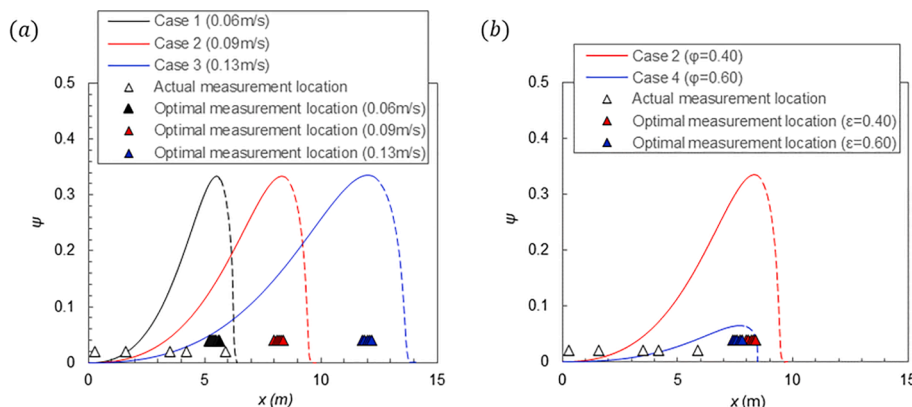

Fig. A.3. Pipe profiles of the determinant of the FIM of the four cases listed in Table 2. Subfigure (a) demonstrates the effect of the mixture velocity at a constant oil fraction of 0.40, while subfigure (b) illustrates the effect of the oil fraction at a constant mixture velocity of 0.09 m s^{-1}.

potential of employing PSA as a means to improve the overall effectiveness of the data collection process, ultimately resulting in more precise parameter estimates.

Plots illustrating the determinant of the FIM against pipe length have also been generated and are shown in Fig. A.3 of the Appendix. A comparison of the results in Fig. A.3 and those presented in Fig. 6 reveals that there is less than 3% difference in peak position between the trace and the determinant.

5.3. Experiment design for parameter precision

Model-based design of experiments in gPROMS ModelBuilder can be used to recommend experiments to improve the precision of the estimates of C_h and r_V^*. During experimental design, the internal diameter of the pipe was fixed at 0.1 m, consistent with the experimental setup described in Section 3. Additionally, the drop size in the inlet was set to 0.25 mm. The lower and upper limits for the mixture velocity u_M were defined as 0.03 m s^{-1} and 0.30 m s^{-1}, respectively, while the oil fraction varied between 0.1 and 0.6, to ensure that water-continuous dispersions are formed. The initial guess for u_M was chosen as 0.06 m s^{-1} which, out of the mixture velocities studied during PSA, this value moved the peak of the sensitivity curve closer to the inlet, as shown in Fig. 6(a). Similarly, the initial estimate for the oil fraction was set to 0.4, since it was

observed that Case 2 with $\varphi_0 = 0.4$ in Fig. 6(b) resulted to a higher peak ψ_{max} in the sensitivity. It is worth noting that sequential MBDoE was performed, hence prior experiments conducted by Pereyra et al. (2013) were taken into consideration during experiment design, and information available from those runs was incorporated into experiment design.

Optimisation of the length of the test section was performed, setting the lower and upper bounds to 4 m and 6 m respectively. An initial guess of 5.5 m was selected for the length. Consistent with experiments performed by Pereyra et al. (2013), measurements were planned to be taken at five distinct locations. The initial guesses for the measurement locations were set as 0.3 m, 1.6 m, 3.5 m, 4.2 m, and 5.0 m, with the intention of optimising these locations. A constraint of a minimum distance of 0.1 m between the measuring locations was imposed. The optimisation process was repeated three times, using each of the A-, D-, and E-optimal criteria to enable comparison.

The initial guesses, and the lower and upper bounds of the controlled variables and the initial conditions used for model-based experiment design are outlined in Table 5, along with the optimal values obtained with each of the A-, D-, and E-optimal criteria. The optimal measuring locations obtained with each criterion are presented in Table 6. All three criteria yielded nearly identical results, which also satisfied the *t*-test. The experimental design was repeated using different initial guesses for design variables, without any improvement in the uncertainty of the

model parameters.

The MBDoE results suggest that utilising an oil fraction of 0.22 and a mixture velocity of 0.076 m s^{-1} is recommended. The optimal measurement locations for these specific conditions, as presented in Table 6, are clustered around a single location. This aligns with PSA findings in Fig. 6, where the optimal measurement locations cluster around the point of highest sensitivity. Furthermore, the measurement locations are situated near the end of the pipe, closely resembling the PSA findings for Case 1 where the mixture velocity was 0.06 m s^{-1}. Similarly to PSA results, a constant measurement interval of 0.1 m is recommended, which corresponds to the minimum allowable distance between measurements.

The parameter statistics can be found in Table 7. Notably, the 95% *t*-values are 3.9 for both C_h and r_V^* using either criterion, surpassing the reference *t*-value of 1.68. Therefore, a significant improvement in parameter precision is expected compared to their previous values listed in Table 3, particularly for the *t*-value of C_h, which has doubled in magnitude.

Fig. 7 shows a comparison between the confidence ellipses resulting from the initial parameter estimation performed in Section 5.1 and the expected confidence ellipses obtained using the three optimisation criteria. Each confidence ellipse was plotted for the 95% confidence interval. The results demonstrate that MBDoE is expected to consistently improve parameter precision, irrespective of the chosen criterion, thus enhancing the reliability of parameter estimates.

As anticipated, the three criteria yielded remarkably similar outcomes, indicating comparable performance. The optimisation criteria exhibited substantial improvements in the expected confidence region of the parameter estimates. This enhancement is clearly demonstrated by the significant reduction in the area of the ellipse, which signifies a reduction in uncertainty and an increased level of confidence in the estimated parameters.

After conducting the newly designed experiments, it is essential to recalibrate the model. If the precision of the parameters following recalibration is still not satisfactory, the experiment design process can be repeated using the new parameter estimates. Sequential MBDoE is an iterative process that provides predictions based on the current knowledge about the system.

6. Conclusions

A parametric study has been conducted on the model outlined in Evripidou et al. (2022) for the prediction of the separation of dispersed liquid–liquid pipe flows, with the aim to enhance the accuracy of existing models. By leveraging experimental data sourced from Pereyra et al. (2013), parameter estimation, parametric sensitivity analysis, and model-based design of experiments (MBDoE) techniques are employed to propose an effective framework for acquiring precise parameter estimates for mechanistic models of separating dispersions.

Parameter estimation showed that the four experimental datasets obtained from Pereyra et al. (2013) were sufficient for estimating the coalescence coefficient r_V^* with a high precision. However, the information content associated with the settling coefficient C_h was not enough to estimate this parameter precisely. The study also revealed that C_h greatly influences the predictions of the model, particularly in drop settling-controlled regions, emphasising the need for a more precise parameter estimate. Parametric sensitivity analysis identified a peak in the trace of the FIM, ψ_{max}, near the point of depletion of the dense-packed layer. This peak indicates the most parametrically sensitive pipe location, i.e. the location where the information content of the measurements for their use in the parameter estimation is maximised. It was demonstrated that the location and magnitude of ψ_{max} are altered through manipulation of the controlled variables and the initial conditions. Specifically, it was shown that a decrease in the mixture velocity u_M shifts the peak towards the inlet without affecting the magnitude of the peak. However, a relationship between the dispersed phase fraction φ_0 and either the location or the magnitude of ψ_{max} could not be established. Finally, experiment design for parameter precision using either of the A-, D-, and E- optimal criteria yielded nearly identical proposed experiments. All criteria successfully led to anticipated improvements in the precision of the parameter estimates, as evidenced by the substantial increase in the *t*-values.

The findings of this study highlight the potential of both parametric sensitivity analysis and MBDoE techniques to enhance the accuracy of mechanistic models for separating dispersions. These approaches enable the precise estimation of uncertain parameters, thereby increasing the overall accuracy of the model predictions. By leveraging PSA and MBDoE, the experimental design process can be optimised, allowing for more informed and efficient data collection. The proposed methods streamline the optimisation of experimental design, eliminating the need for iterative trial and error approaches, resulting in significant savings in time and resources, ultimately serving as a valuable guide for future experimental work.

Appendix

A.1 Nomenclature

Latin	
A	Cross-sectional area (m^2)
Ar	Archimedes number (-)
C_1, C_2	Coefficients obtained on the basis of continuity (-)
C_h	Hindered settling coefficient (-)
CI	Confidence interval
C_w	Modified friction coefficient (-)
d	Diameter (m)

(continued on next page)

(*continued*)

Latin	
g	Gravitational acceleration (m s^{-2})
H	Hamaker coefficient (N m)
h	Layer thickness (m)
$\widetilde{h}_P$	Drop-packing height (m)
ID	Internal diameter of the pipe (m)
K_{HR}	Hadamard-Rybczynski factor (-)
La	Modified Laplace number (-)
N	Number of measured responses
N_θ	Number of parameters
n_ϕ	Number of design variables
$r_{\mathrm{F,C}}$	Drop-drop contact radius (m)
$r_{\mathrm{F,I}}$	Drop-interface contact radius (m)
r_V^*	Dimensionless asymmetry coefficient (-)
r_α	Channel contour radius (m)
sf	Scaling factor
t_i	t-value for the i-th model parameter
t_{ref}	Reference t-value
u	Velocity (m s^{-1})
$v_{\theta,i}$	Estimated variance for the i-th model parameter
x	Displacement in the axial direction of the flow downstream of the inlet (m)
$\overline{x}$	Length of depletion of the settling layer (m)
$\overline{\overline{x}}$	Length of depletion of the dense-packed layer (m)
y	Vertical displacement from the bottom of the pipe (m)
y_i	i-th predicted response
Greek	
γ	Interfacial tension (N m^{-1})
ε	Infinitesimally small perturbation in parameter i
θ_i	i-th model parameter
λ	Flotation parameter (-)
μ	Viscosity (Pa s)
ξ	Flotation parameter (-)
ρ	Density (kg m^{-3})
τ_{C}	Drop-drop coalescence time (s)
τ_{I}	Drop-interface coalescence time (s)
φ	Dispersed-phase fraction (-)
$\overline{\varphi}_P$	Average holdup in the dense-packed layer (-)
χ_i^2	Chi-square statistic for the i-th model parameter
χ_{ref}^2	Reference Chi-square
Superscripts & Subscripts	
$+$	Dimensionless variable
0	Initial
C	Continuous phase
D	Initially dispersed phase
I	Interface
M	Mixture
P	Dense-packed layer
p	Drop
pipe	Pipe
S	Settling
sep	Separation
Vectors & Matrices [dimension]	
$\mathbf{D}$	Matrix of eigenvalues $[N_\theta \times N_\theta]$
$\mathbf{H}_\theta$	Fisher information matrix $[N_\theta \times N_\theta]$
$\mathbf{Q}$	Sensitivity matrix $[N_\theta \times N_\theta]$
$\mathbf{V}_\theta$	Variance-covariance matrix of model parameters $[N_\theta \times N_\theta]$
$\mathbf{v}_\theta$	Matrix of eigenvectors $[N_\theta \times N_\theta]$
$\mathbf{\Sigma_y}$	Variance-covariance matrix of measurement errors $[N_\theta \times N_\theta]$
$\mathbf{\phi}$	Design vector $[n_\phi]$
$\mathbf{\phi_{opt}}$	Optimal design vector $[n_\phi]$

A.2 Mechanistic model

A.2.1 Settling velocity

In the correlation for the settling velocity of drops in Eq. (2), the two dimensionless settling parameters are given by

$$\lambda = \frac{1 - \varphi_{\mathrm{S}}}{2\varphi_{\mathrm{S}}\mathrm{K}_{\mathrm{HR}}} \exp\left(\frac{2.5\varphi_{\mathrm{S}}}{1 - 0.61\varphi_{\mathrm{S}}}\right) \tag{A1}$$

and

$$\xi = 5K_{HR}^{-\frac{3}{2}}\left(\frac{\varphi_S}{1-\varphi_S}\right)^{0.45}. \tag{A2}$$

Additional dimensionless numbers include the Archimedes number, Ar, which can be calculated by

$$Ar = \frac{\rho_C \Delta\rho g d_p^3}{\mu_C^2} \tag{A3}$$

with g being the gravitational constant, the Hadamard-Rybczynski factor, K_{HR}, given by

$$K_{HR} = \frac{3(\mu_C + \mu_D)}{2\mu_C + 3\mu_D}, \tag{A4}$$

the modified friction coefficient, denoted as C_W, calculated by

$$C_w = \frac{Ar}{6Re_\infty^2} - \frac{3}{K_{HR}Re_\infty}, \tag{A5}$$

and the Reynolds number of a single drop moving vertically in an infinite medium, Re_∞, which according to Ishii and Zuber (1979) can be obtained by

$$Re_\infty = 9.72\left[(1 + 0.01Ar)^{\frac{4}{7}} - 1\right], \tag{A6}$$

A.2.2 Coalescence times

In the coalescence time correlations presented in Eqs. (7) and (8), γ denotes the interfacial tension between the two phases, and H represents the Hamaker coefficient. Henschke et al. (2002) proposed a value of 10^{-20} N m for the Hamaker coefficient for any system.

$r_{F,C}$ is the drop-drop contact area radius given by

$$r_{F,C} = 0.3025d_p\sqrt{1 - \frac{4.7}{La + 4.7}}, \tag{A7}$$

$r_{F,I}$ is the drop-interface contact area radius and can be linked to $r_{F,C}$ using

$$r_{F,I} = \sqrt{3}r_{F,C} \tag{A8}$$

and r_a is the radius of the channel contour formed as three drops approach and is calculated by

$$r_\alpha = 0.5d_p\left(1 - \sqrt{1 - \frac{4.7}{La + 4.7}}\right). \tag{A9}$$

La is a modified Laplace number, given by

$$La = \left(\frac{|\rho_C - \rho_D|g}{\gamma}\right)^{0.6}\widetilde{h}_P^{\ 0.2}d_p. \tag{A10}$$

La represents hydrostatic pressure-to-interfacial tension ratio, and accounts for drop packing. The hydrostatic pressure arises from the drop-packing height beneath the draining film, denoted as $\widetilde{h}_P$. Consequently, $\widetilde{h}_P$ corresponds to the DPL thickness if one exists. When there is no DPL, the settling layer directly contacts the oil layer. In this scenario, Evripidou et al. (2022) suggest that $\widetilde{h}_P$ is considered equal to the drop size at the interface $d_{p,I}$.

A.2.3 Dense-packed layer

At any given length in the *four-layer* flow regime, the cross-sectional area of the DPL is given by

$$A_P = \frac{A_{pipe}(\varphi_0 - \varphi_S) - A_D(1 - \varphi_S) + A_C\varphi_S}{\varphi_P - \varphi_S} \tag{A11}$$

where ε_P is the average dispersed-phase fraction in the DPL given by

$$\varphi_P = \frac{\varphi_S + \varphi_I}{2} \tag{A12}$$

as suggested by Henschke et al. (2002).The oil fraction at the coalescing interface φ_I is approximated by 0.9 as proposed by Evripidou et al. (2022). In the case of depletion of the SL (i.e. in the *3-layer with DPL* flow regime) Eq. (A11) simplifies to

$$A_P = \frac{A_{pipe}\varphi_0 - A_D}{\varphi_P}. \tag{A13}$$

Following the depletion of the SL, the average holdup in the DPL $\overline{\varphi}_P$ is allowed to increase from its previous value and is calculated by

$$\overline{\varphi}_P = \varphi_I - exp\left(-C_1\frac{x}{u_M} - C_2\right). \tag{A14}$$

Coefficients C_1 and C_2 are determined to satisfy the continuity condition that at $x = \overline{x}, \varphi_P = \overline{\varphi}_{P|\overline{x}}|_{\overline{x}}$, hence

$$C_1 = \frac{\overline{\varphi}_P|_{\overline{x}}^2 \psi}{\left(A_{pipe}\varphi_0 - A_D\right)\left(\varphi_I - \overline{\varphi}_P|_{\overline{x}}\right)}. \tag{A15}$$

and

$$C_2 = -C_1\frac{\overline{x}}{u_M} - \ln\left(\varphi_I - \overline{\varphi}_P|_{\overline{x}}\right), \tag{A16}$$

where, according to Pereyra et al. (2013)

$$\psi = \left[\frac{\partial A_P}{\partial h_P}\left(u_s + u_M\frac{dh_D}{dx}\right) - \frac{u_M}{\overline{\varphi}_P|_{\overline{x}}}\frac{\partial A_D}{\partial h_D}\frac{\partial h_D}{\partial x} - u_M\frac{\partial A_P}{\partial h_D}\frac{\partial h_D}{\partial x}\right]_{x=\overline{x}}. \tag{A17}$$

Depletion of the DPL occurs if h_P becomes smaller than $d_{P,I}$, as suggested by Evripidou et al. (2022). In that case Eq. (A11) reduces to

$$A_P = 0. \tag{A18}$$

At this point, the SL makes contact with the pure oil layer and a monolayer of drops replaces the DPL.

A.2.4 Settling layer/oil layer interface

In the presence of a DPL, the oil fraction at the coalescing interface, φ_I, is assumed to be 0.9. In the case of the *3-layer with SL* flow regime, where the SL is in contact with the oil layer, the value of φ_I is determined by

$$\varphi_I = \frac{A_{pipe}\varphi_0 - A_D - A_S\varphi_S}{A_I}. \tag{A19}$$

When the thickness of the settling layer decreases to a value smaller than the drop diameter, the oil fraction at the interface is equivalent to the remaining oil fraction in the dispersion, hence

$$\varphi_I = \frac{A_{pipe}\varphi_0 - A_D}{A_S}. \tag{A20}$$

A.2.5 Geometric equations

The cross-sectional area of the pure water layer is given by

$$A_C = \frac{ID^2}{4}\left[\pi - \cos^{-1}(\omega_C) + (\omega_C)\sqrt{1 - \omega_C^2}\right], \tag{A21}$$

where $\omega_C = \frac{2h_C}{ID} - 1$. The cross-sectional area of the oil layer is

$$A_D = \frac{ID^2}{4}\left[\pi - \cos^{-1}(\omega_D) + (\omega_D)\sqrt{1 - \omega_D^2}\right], \tag{A22}$$

where $\omega_D = \frac{2h_D}{ID} - 1$, and its partial derivative is

$$\frac{\partial A_D}{\partial h_D} = 2\sqrt{h_D(ID - h_D)} \tag{A23}$$

The area of the DPL is determined by

$$A_P = \frac{ID^2}{4}\left[\pi - \cos^{-1}(\omega_D) + (\omega_D)\sqrt{1 - \omega_D^2}\right] - A_D, \tag{A24}$$

where $\omega_P = \frac{2h_P}{ID} - 1$, and its partial derivative by

$$\frac{\partial A_P}{\partial h_P} = 2\sqrt{(h_D + h_P)(ID - h_P - h_D)}. \tag{A25}$$

$\frac{\partial A_P}{\partial h_D}$ is given by the difference between $\frac{\partial A_P}{\partial h_P}$ and $\frac{\partial A_D}{\partial h_D}$, as

$$\frac{\partial A_P}{\partial h_D} = \frac{\partial A_P}{\partial h_P} - \frac{\partial A_D}{\partial h_D} = 2\sqrt{(h_D + h_P)(ID - h_P - h_D)} - 2\sqrt{h_D(ID - h_D)}. \tag{A26}$$

In the *3-layer with SL* flow regime, the area of the monolayer of drops found along the coalescing interface calculated by

$$A_I = \frac{ID^2}{4}\left[\pi - \cos^{-1}(\omega_I) + (\omega_I)\sqrt{1-\omega_I^2}\right] - A_I, \tag{A27}$$

where $\omega_I = \frac{2d_p}{ID} - 1$. Finally, the area of the SL is obtained through a mass balance on the pipe cross-section:

$$A_S = ID - A_D - A_C - A_P. \tag{A28}$$

A.2.6 Table summarising model equations
    See Table A.3

A.3 Parametric sensitivity analysis

The local sensitivities were calculated according to Eq. (11) and inserted in the sensitivity matrix, which becomes

$$\mathbf{Q}(C_h, r_V^*) = \begin{bmatrix} \dfrac{\partial y_C}{\partial C_h} & \dfrac{\partial y_C}{\partial r_V^*} \\[2ex] \dfrac{\partial y_D}{\partial C_h} & \dfrac{\partial y_D}{\partial r_V^*} \end{bmatrix}. \tag{A29}$$

It follows that the elements of the FIM $\mathbf{H}_\theta$ are

$$\mathbf{H}_{11}(C_h, r_V^*) = \sigma_{11}^{-2}\left(\frac{\partial y_C}{\partial C_h}\right)^2 + \sigma_{22}^{-2}\left(\frac{\partial y_D}{\partial r_V^*}\right)^2, \tag{A30}$$

$$\mathbf{H}_{12}(C_h, r_V^*) = \mathbf{H}_{21}(C_h, r_V^*) = \sigma_{11}^{-2}\left(\frac{\partial y_C}{\partial C_h}\right)\left(\frac{\partial y_C}{\partial r_V^*}\right) + \sigma_{22}^{-2}\left(\frac{\partial y_D}{\partial C_h}\right)\left(\frac{\partial y_D}{\partial r_V^*}\right), \tag{A31}$$

and

$$\mathbf{H}_{22}(C_h, r_V^*) = \sigma_{11}^{-2}\left(\frac{\partial y_C}{\partial r_V^*}\right)^2 + \sigma_{22}^{-2}\left(\frac{\partial y_D}{\partial r_V^*}\right)^2. \tag{A32}$$

A.4 Confidence interval of $\mathbf{r}_V^*$

A.5 Fisher information analysis

References

Balmelli, M., Steiner, L., Hartland, S., 2000. Behaviour of turbulent dispersions in a stirred single-stage cell. Chem. Eng. Sci. 55, 1653–1660.

Bard, Y., 1977. Nonlinear Parameter Estimation. Academic Press, New York, USA.

Bhardwaj, A., Hartland, S., 1994. Kinetics of coalescence of water droplets in water-in-crude oil emulsions. J. Dispers. Sci. Technol. 15 (2), 133–146.

Draper, N.R., Smith, H., 1998. Applied Regression Analysis, Vol. 326. John Wiley & Sons.

Evripidou, N., Voulgaropoulos, V., Angeli, P., 2019. Simplified mechanistic model for the separation of dispersed oil-water horizontal pipe flows. BHR 19th International Conference on Multiphase Production Technology. BHR Group.

Evripidou, N., Avila, C., Angeli, P., 2022. A mechanistic model for the prediction of flow pattern transitions during separation of liquid-liquid pipe flows. Int. J. Multiph. Flow 104172.

Franceschini, G., Macchietto, S., 2008. Model-based design of experiments for parameter precision: State of the art. Chem. Eng. Sci. 63 (19), 4846–4872.

Frising, T., Noik, C., Dalmazzone, C., 2006. The liquid/liquid sedimentation process: from droplet coalescence to technologically enhanced water/oil emulsion gravity separators: A review. J. Dispers. Sci. Technol. 27, 1035–1057.

Galvanin, F., Ballan, C.C., Barolo, M., Bezzo, F., 2013. A general model-based design of experiments approach to achieve practical identifiability of pharmacokinetic and pharmacodynamic models. J. Pharmacokinet Pharmacodyn. 40, 451–467.

Henschke, M., Schlieper, L.H., Pfennig, A., 2002. Determination of a coalescence parameter from batch-settling experiments. Chem. Eng. J. 85 (2–3), 369–378.

Hines, W.W., Montgomery, D.C., Goldsman, D.M., Borror, C.M., 2003. Probability and statistics in engineering, fourth ed. Wiley, New York.

Huang, C., Cattani, F., Galvanin, F., 2023. An optimal experimental design strategy for improving parameter estimation in stochastic models. Comput. Chem. Eng. 170, 108133.

Jeelani, S.A.K., Benoist, G., Joshi, K.S., Gunde, R., Kellenberger, D., Windhab, E. J., (2005a). Creaming and aggregation of particles in suspensions. Colloids and Surfaces A: Physicochemical and Engineering Aspects, 263(1-3), 379-389.

Jeelani, S.A.K., Hartland, S., (1986b). Scale-up of industrial gravity settlers from batch settling data. Proceedings of the International Solved Extraction Conference ISEC`86, Munich; Vol. 3, 453–460.

Ishii, M., Zuber, N., 1979. Drag coefficient and relative velocity in bubbly, droplet or particulate flows. AIChE journal 25 (5), 843–855.

Jeelani, S.A.K., Hartland, S., 1986a. Prediction of dispersion height in liquid/liquid gravity settlers from batch settling data. Chem. Eng. Res. Des. 64, 450–460.

Jeelani, S.A.K., Hartland, S., 1988. Dynamic response of gravity settlers to changes in dispersion throughput. AIChE J 34 (2), 335–340.

Jeelani, S.A.K., Hartland, S., 1993. The continuous separation of liquid/liquid dispersions. Chem. Eng. Sci. 48 (2), 239–254.

Jeelani, S.A.K., Hosig, R., Windhab, E.J., 2005b. Kinetics of low Reynolds number creaming and coalescence in droplet dispersions. AIChE J. 51 (1), 149–161.

Jeelani, S.A.K., Pandit, A., Hartland, S., 1990. Factors affecting the decay of batch liquid-liquid dispersions. Can. J. Chem. Eng. 68, 924–931.

Jeelani, S.A.K., Panoussopoulos, K., Hartland, S., 1999. Effect of turbulence on the separation of liquid-liquid dispersions in batch settlers of different geometries. Ind. Eng. Chem. Res. 38, 491–501.

Joshi, M., Kremling, A., Seidel-Morgenstern, A., 2006. Model based statistical analysis of adsorption equilibrium data. Chem. Eng. Sci. 61 (23), 7805–7818.

Krausch, N., Barz, T., Sawatzki, A., Gruber, M., Kamel, S., Neubauer, P., Cruz Bournazou, M.N., 2019. Monte Carlo simulations for the analysis of non-linear parameter confidence intervals in optimal experimental design. Front. Bioeng. Biotechnol. 7, 122.

Lobo, L., Ivanov, I., Wasan, D., 1993. Dispersion coalescence: Kinetic stability of creamed dispersions. AIChE J. 39 (2), 322–334.

Mason, S.L., May, K., Hartland, S., 1995. Drop size and concentration profile determination in petroleum emulsion separation. Colloids Surf. A 96, 85–92.

Noïk, C., Palermo, T., Dalmazzone, C., 2013. Modeling of liquid/liquid phase separation: application to petroleum emulsions. J. Dispers. Sci. Technol. 34 (8), 1029–1042.

Panoussopoulos, K., Hartland, S., Gramme, P.E., Sontvedt, T., 1997. Drop size and hold-up profiles in the separation of crude oil-water dispersions. Paper Presented at International Symposium on Liquid-Liquid Two-Phase Flow and Transport Phenomena.

Pereyra, E., Mohan, R., Shoham, O., 2013. A simplified mechanistic model for an oil/water horizontal pipe separator. Oil and Gas Facilities 2 (03), 40–46.

Perry, R.H., Green, D.W., Maloney, J.O., 1997. Perry's handbook of chemical engineering. Perry's Handbook of Chemical Engineering.

Pilehvari, A., Saadevandi, B., Halvaci, M., Clark, P.E., 1988. Oil/water emulsions for pipeline transport of viscous crude oils. SPE Annual Technical Conference and Exhibition. Onepetro.

Pukelsheim, F., 1993. Optimal Design of Experiments. J Wiley & Sons, New York, USA.

Quaglio, M., Waldron, C., Pankajakshan, A., Cao, E., Gavriilidis, A., Fraga, E.S., Galvanin, F., 2019. An online reparametrisation approach for robust parameter estimation in automated model identification platforms. Comput. Chem. Eng. 124, 270–284.

Saltelli, A., Chan, K., Scott, E.M., 2009. Sensitivity Analysis. Wiley Series in Probability and Statistics. John Wiley & Sons.

Schenkendorf, R., Xie, X., Rehbein, M., Scholl, S., Krewer, U., 2018. The impact of global sensitivities and design measures in model-based optimal experimental design. Processes 6 (4), 27.

Skjefstad, H., Stanko, M., 2019. Experimental performance evaluation and design optimization of a horizontal multi-pipe separator for subsea oil-water bulk separation. J. Pet. Sci. Eng. 176, 203–219.

Voulgaropoulos, V., Jamshidi, R., Jamshidi, R., Angeli, P., 2019. Experimental and numerical studies on the flow characteristics and separation properties of dispersed liquid-liquid flows. Phys. Fluids 31 (7), 073304.

Walter, E., Pronzato, L., 1997. Identification of parametric models: From experimental data. Springer-Verlag, Berlin.

Wang, Z.M., Zhang, J., 2016. Corrosion of multiphase flow pipelines: the impact of crude oil. Corros. Rev. 34 (1–2), 17.